Received July 2, 2021, accepted August 1, 2021, date of publication August 11, 2021, date of current version August 20, 2021.

Digital Object Identifier 10.1109/ACCESS.2021.3104011

Controlled Scaffold Platform Designs on Nasopharyngeal Carcinoma Cell Separation

MUTING WANG AND STELLA W. PANG, (Fellow, IEEE)
Department of Electrical Engineering, City University of Hong Kong, Hong Kong, China
Centre for Biosystem, Neuroscience, and Nanotechnology, City University of Hong Kong, Hong Kong, China

Corresponding author: Stella W. Pang (pang@cityu.edu.hk)

This work was supported in part by the Center for Biosystems, Neuroscience, and Nanotechnology of City University of Hong Kong under Grant 9360148 and Grant 9380082; and in part by the University Grants Council of Hong Kong under General Research Fund for Project 11218017, Project 11213018, Project 11212519, and Project 11207620.

ABSTRACT Nasopharyngeal carcinoma (NPC) is a highly invasive and metastatic disease occurring in the nasopharynx. For early diagnosis or treatment, it is helpful to separate invasive nasopharyngeal carcinoma (NPC43) cells from epithelial (NP460) cells. However, the lack of proper *in vivo* models significantly hinders the systematic study of NPC. In this study, an *in vitro* two-layer scaffold platform was developed to mimic the extracellular matrix of the tissue that allows the investigation of carcinoma and epithelial cell migration behaviors. Three precisely controlled factors were designed to investigate how topographic cues affected migration of NP460 and NPC43 cells: overlay angles between the top and bottom layers, top layer thicknesses, and surface topography of the bottom layer ridges. These designs offered different surface contact areas for cells to probe and form focal adhesions as they migrated on the platforms. As NP460 and NPC43 cells respond differently to the surrounding microenvironments, when the top layers were perpendicular to the bottom layers, 66.3% NPC43 cells could move into the 10 μm wide trenches compared to 5.5% for NP460 cells. However, NP460 and NPC43 cells migrating into top layer trenches were hindered when the top layer was too shallow or too thick. Moreover, the gratings added on the bottom layer ridges promoted cells to squeeze into the trenches. These results yielded over 92.3% separation efficiency on platforms with a 15-μm thick top layer being perpendicular to the bottom layer and gratings on the bottom layer ridges.

INDEX TERMS Nasopharyngeal carcinoma (NPC), two-layer scaffold platform, cell separation, cell migration.

I. INTRODUCTION

Cancer is one of the global leading causes of death and a major obstacle in extending life expectancy. In 2020, it was estimated that there were 19.3 million new cases of cancer and nearly 10 million cancer deaths worldwide [1]. Early cancer diagnosis and improved cancer therapy using technological innovations are important and helpful for cancer patients. For instance, leukemia can be detected early by isolating leukemia cells from the blood, thereby providing valuable biological information for cancer treatment [2]. In tissue engineering, specific cells are identified and purified, then used to form the desired tissue [3]. Overall, the separation of cancer cells from normal cells helps improve the characterization of cell phenotype, diagnostic accuracy, and therapeutic efficacy [4].

The nasopharynx is a small tubular structure above the soft palate that connects the nose to the oropharynx [5]. Nasopharyngeal carcinoma (NPC) is a highly invasive tumor in the nasopharynx. NPC is more common in certain regions of North Africa, Middle East, and Asia, particularly southeast China [5]–[9]. The etiology of NPC is complex and has not yet been fully understood. It is caused by multiple factors such as viruses, environmental influences, and genetics. The primary influence is strongly associated with infection by the Epstein-Barr virus (EBV) [10]–[13]. In general, it is difficult to establish NPC cell lines or animal models that are EBV positive [14]–[16].

Existing cell separation technologies can be divided into two categories. The first is based on physical criteria, such

The associate editor coordinating the review of this manuscript and approving it for publication was Taous Meriem Laleg-Kirati.

as differences in cell size, shape, and density, and involves technologies for filtration and centrifugation [17]. However, they are disadvantaged by low specificity and scale-up issues. The other category includes affinity methods based on cell surface and biophysical characteristics, such as fluorescence-activated cell sorting and magnetic cell sorting [18], [19]. Furthermore, microfluidic systems for cell separation have been used in recent years. Their advantages include low sample volume, high sensitivity, and higher portability [20].

Cell migration involves the movement of a single cell or collective cells in response to mechanical or chemical signals [21]. It is a primary cellular process that occurs continuously, sometimes leading to the progression of pathogenic diseases [22]. Previous studies reported cell migration behaviors on two-dimensional (2D) platforms with various engineered topographies [23]–[30]. However, 2D models do not accurately represent the microenvironment of tumors *in vivo*. With the additional vertical dimension, three-dimensional (3D) models can better reflect the microenvironment of living tissue in size, structure, and cell polarity [31]–[33]. While cell migration is important in maintaining tissue health and homeostasis, unwanted migratory events are undesirable and can lead to metastatic cancer and inflammatory disease [22], [34]. Therefore, understanding cell migration is an important step in developing disease treatment.

It is difficult to observe cell separation, invasion behaviors, and viability at the same time based on existing cell screening methods. For example, microfluidic devices have been used for high throughput cell screening. Although microfluidic devices provide a controlled physical and chemical environment, the work mostly focuses on the lateral migration of cells [35]. With our proposed platforms, NPC cell separation efficiency could be monitored through tracking the traversing behaviors of NPC cells into narrow trenches from the top layer, which could be observed using bright field microscopy without additional complex immunofluorescence staining [32], [35]. In addition, tracking of single cell movement could be achieved, which provides a rapid and convenient way to analyze cell migration behaviors.

The extracellular matrix (ECM) serves as a scaffold structure for cells in tissues. It consists of a 3D network of fiber-forming proteins, such as collagen, laminin, and fibronectin. Using a transmission electron microscope (TEM), the cross-striated pattern of native collagen fibrils could be observed [36]. The diameter of the ECM fiber is tissue-specific and changes due to aging, fibrosis, or cancer, affecting tissue organization and function. Moreover, two patterns of fibril organization were observed by TEM. One is the regular angle shift in fibril orientation from one to another, with alternating parallel and orthogonal fibers. The other one is an arced structure [36]. The geometry and dimensions of the scaffold have big impacts on cell adhesion and migration [37]. Based on these findings, a two-layer scaffold platform with three tunable factors was established, including overlay angles between the top and bottom layers, the trench depth of the top layer, and the topography on the bottom layer ridges, for cell separation.

Herein, a two-layer scaffold platform was developed to mimic the ECM in the tissue. Using the microfabrication technologies, three designed elements were precisely controlled to form different surface contact areas for studying cell migration. In this study, platforms were developed based on previous studies to mimic the physical properties of the ECM and to further investigate how these physical properties influence cell adhesion and migration. Nasopharyngeal epithelial (NP460) and carcinoma (NPC43) cells were used and their movements were observed in real-time. The discrepancies of NP460 and NPC43 cells in cell motility, morphology, and traversing behaviors were examined. The scaffold platform was optimized to effectively separate NPC43 cells from NP460 cells. This result could potentially be used as a basis to develop early diagnosis and treatment methods for NPC tumors.

II. EXPERIMENT AND METHODS

A. FABRICATION TECHNOLOGY OF TWO-LAYER SCAFFOLD PLATFORMS

The fabrication technology of two-layer scaffold platforms is shown in Fig. 1. Figure 1(a) shows the formation of the bottom layer. By deep reactive-ion etching with SPR6112R positive photoresist as an etch mask, a silicon (Si) stamp with a 15 μm deep grating was first fabricated. The Si stamp was then coated with trichloro (1H, 1H, 2H, 2H-perfluorooctyl) silane (FOTS) and baked for 20 min at 80 °C, which resulted in a low surface energy of 16±0.3 mN/m to promote easy demolding of polydimethylsiloxane (PDMS). PDMS was prepared by mixing PDMS prepolymer and curing agent (Dow Corning Sylgard 184 Kit) at a 10:1 ratio. The PDMS was casted on the Si stamp and baked for 6 h at 80 °C. The bottom layer was formed by peeling off the cured PDMS replica from the Si stamp.

The top layer of the scaffold platform was formed by imprint lithography under 3×10^4 Torr for 5 min at 130 °C so that the grating structure could be transferred from a Si stamp to a PDMS layer on the Si substrate, as shown in Fig. 1(b). Before PDMS coating, the Si substrate was coated with a mixture of 3-methacryloxypropyltrichlorosilane and FOTS in a 4:1 ratio and baked for 2 h at 80 °C. This saline mixture provided a higher surface energy of 20±0.6 mN/m compared to FOTS, which allowed the patterned PDMS to stay on the Si substrate but released from the Si stamp. The Si stamp consisted of 15 μm deep gratings coated with FOTS. The imprinted top layer was placed on a hot plate for 3 min at 120 °C to cure the PDMS. After imprinting, reactive-ion etching was applied using 5/20 sccm O_2/SF_6, 10 mTorr pressure, and 250 W RF power for 5 min to remove the residual PDMS layer on the imprinted top layer. The imprinted top layer was aligned with a 30°, 60°, and 90° offset from the bottom layer. To bond the two layers together, an O_2/N_2 plasma was applied with 400/400 sccm O_2/N_2, 150 mTorr or mbar pressure, and 200 W RF power for 75 s, followed by baking

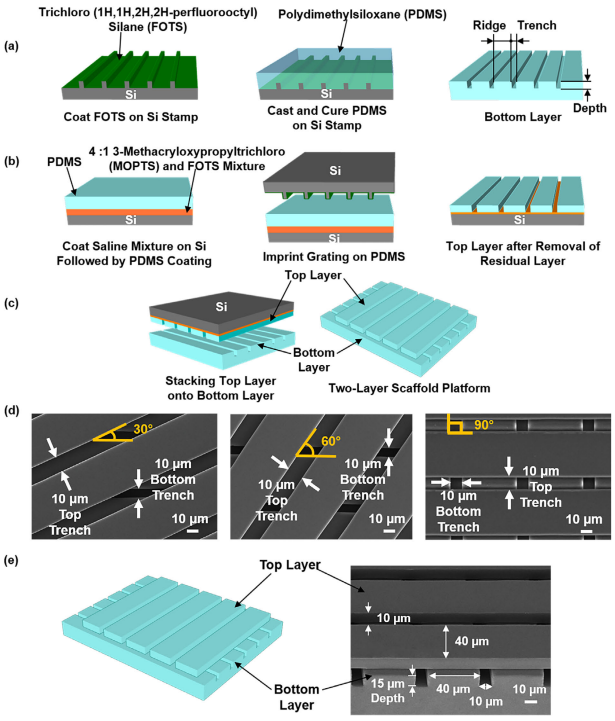

FIGURE 1. Fabrication technology of two-layer scaffold platform. (a) Bottom layer was obtained by demolding PDMS from Si stamp. (b) Top layer was fabricated by imprinting grating structure to Si substrate. (c) Stacking two layers after O_2 plasma to form scaffold platform. (d), (e) Micrographs of two-layer scaffold platforms with overlay angles of 30°, 60°, and 90°. Both top and bottom layers were gratings with 40 μm wide ridges, 10 μm wide trenches, and 15 μm deep.

on a hot plate for 10 min at 80 °C, as shown in Fig. 1(c). After the O_2/N_2 plasma, the PDMS layers had the higher surface energy of 70±1 mN/m. Figures 1(d-e) show top and side views of the two-layer scaffold platforms with 15 μm deep, 40 μm wide ridges and 10 μm wide trenches. The scaffold platforms with the desired offset angles were placed on 35 mm diameter confocal dishes and treated with an O_2/N_2 plasma to increase the hydrophilicity of the platforms before time-lapse imaging.

B. CELL CULTURE

Immortalized NP460 cells, stably expressing green fluorescent protein fused with LifeAct, and cancerous NPC43 cells, stably expressing Lifeact-mCherry, were used in this study. The immortalized NP460 cells were cultured in a 1:1 mixture of EpiLife medium supplemented with 1% EpiLife defined growth supplement (EDGS, Gibco) and defined keratinocyte serum-free medium supplemented with 0.2% defined keratinocyte growth supplement (Gibco). 1% antibiotic-antimycotic (Gibco, 100 units/ml penicillin G sodium, 100 mg/ml of streptomycin, and 0.25 mg/ml of amphotericin B) was added to the medium. NPC43 cells were cultured in Roswell Park Memorial Institute 1640 medium (1X; Gibco) supplemented with 10% fetal bovine serum (FBS), 1% antibiotic-antimycotic (Gibco, 100 units/ml penicillin G sodium, 100 mg/ml of streptomycin, and 0.25 mg/ml of amphotericin B), and 0.2% 2 mM rock inhibitor Y-27632 (25 mg, ENZO). The cells were kept in an incubator at 37 °C in 5% CO_2, and the medium was changed every two days. These NP460 and NPC43 cells were passaged every three days and cells with over 20 passages were discarded.

C. TIME-LAPSE IMAGING

Plasma with 400/400 sccm O_2/N_2, 150 mTorr pressure, and 200 W RF power for 75 s was applied to clean the 35 mm confocal dish (SDL Life Sciences) and make it hydrophilic. The two-layer scaffold platforms were bonded onto the confocal dish and treated with O_2/N_2 plasma under the same conditions to increase the surface energy, providing a hydrophilic surface for better cell attachment. After the plasma treatment, the platforms were immersed in deionized (DI) water to maintain the hydrophilic surface. 70% ethanol and 1X phosphate-buffered saline (PBS) were used to wash the platforms twice sequentially before cell seeding. 2 ml of NP460 and NPC43 cells with a concentration of 8×10^4 cells/ml were seeded onto the platforms. After 6 h of incubation for initial attachment, cells were evenly distributed on all platforms. Before imaging, the medium in the dish was removed and replaced with a mixture of the culturing medium and CO_2 independent medium (Gibco) with 10% FBS, 1% antibiotic-antimycotic (Gibco, 100 units/ml penicillin G sodium, 100 mg/ml of streptomycin, and 0.25 mg/ml of amphotericin B), and 1% GlutaMAX supplement (100X, Gibco) in 1:1 ratio. The cells were kept at 37 °C and images were captured every 5 min for 16 h by an upright microscope (Nikon Eclipse NI-U).

D. DATA ANALYSIS

Both NP460 and NPC43 cells were tracked by the NIH ImageJ software with a manual tracking plugin (version 1.48). Only live cells that did not contact other cells or were not divided were included in the analysis. Migration trajectories, directionality, and speed of NP460 and NPC43 cells were calculated. Traversing probability was used to indicate the percentage of cells migrated from the top ridges to the 10 μm wide trenches among all the cells. Cells that stayed in the top layer trenches for more than 10 h were counted as traversed cells. Cell solidity was calculated using the cell area divided by the cell convex area. Statistic differences were evaluated using one-way analysis of variance (ANOVA) with post-hoc Tukey HSD test between two or more groups. The results in this paper are presented as mean ± standard error of mean. Each set of experiments were repeated at least three times to ensure reliable results.

E. SCANNING ELECTRON MICROSCOPY

After culturing the cells for 22 h on the scaffold platforms, the cells were washed with 1X PBS twice and immersed in 4% paraformaldehyde for 20 min for fixation. To dehydrate fixed cells, they were immersed in DI water for 10 min and a series of graded ethanol concentrations (30%, 50%, 70%, 80%, 90%, 95%, and 100%) for 5 min for each concentration.

The dehydration process was finished using a critical pointer dryer (EM CPD300, Leica) to transition the ethanol into CO_2. To avoid charging during imaging, a layer of gold was deposited on the samples. The cells morphologies were imaged by a scanning electron microscope (Hitachi SU5000).

III. RESULTS AND DISCCUSION

A. TWO-LAYER SCAFFOLD PLATFORMS FOR CELL CULTURING

A number of microsystems have been developed to study cell migration behaviors [38]–[41]. Most of the systems were complicated and time-consuming to form. In this paper, two-layer scaffold platforms with three precisely controlled elements, including overlay angle between the top and bottom layer, top layer thickness, and topography on bottom layer ridge, were established with the intention to separate NPC43 cells from NP460 cells. These controlled elements were designed to mimic the organization, fibril size, and topography of the ECM. The fabrication technology of the double layer platforms is illustrated in Figs. 1(a-c). The micrographs in Fig. 1(d) demonstrate two layers of grating structures aligned with an overlay angle of 30°, 60°, and 90° between the top and bottom layers, similar to fibrils in the ECM with angle shift [3]. Each layer consisted of a grating with 40 μm wide ridges and 10 μm wide trenches, with a depth of 15 μm, as shown in Fig. 1(e). The dimensions of the grating ridges and trenches were designed to be larger and smaller, respectively, than the typical size of the cells, which is 15– 20 μm [42]. In our previous study, both NP460 and NPC43 cells could hardly move into the 10 μm wide top layer trenches when they were seeded on one-layer platforms with 40 μm wide ridges, 10 μm wide trenches, and 15 μm deep gratings. Nevertheless, with the presence of a bottom layer in a two-layer scaffold platform, more invasive NPC43 cells could squeeze into the 10 μm wide trenches while most of the NP460 cells stayed on the 40 μm wide top ridges. Apart from the overlay angles, the effect of different top layer thicknesses on cell migration behaviors of NP460 and NPC43 cells was also investigated. The thickness of top layers was decisively controlled to be 5, 10, 15, and 30 μm, mimicking fibrils with various dimensions in ECM [3]. Additionally, the effect of the bottom layer surface topography on the traversing probability of NP460 and NPC43 cells was also studied. The aim of using these three controlled components was to provide different surface contact areas for cells to form focal adhesions, and the platforms were optimized to improve cell separation efficiency.

B. TWO-LAYER SCAFFOLD PLATFORMS WITH DIFFERENT OVERLAY ANGLES

1) CELLS TRAJECTORY AND DIRECTIONALITY OF NP460 AND NPC43 CELLS

Previous studies showed that NP460 and NPC43 cells exhibited different migration behaviors when seeded on two-layer scaffold platforms with different dimensions [32], [43].

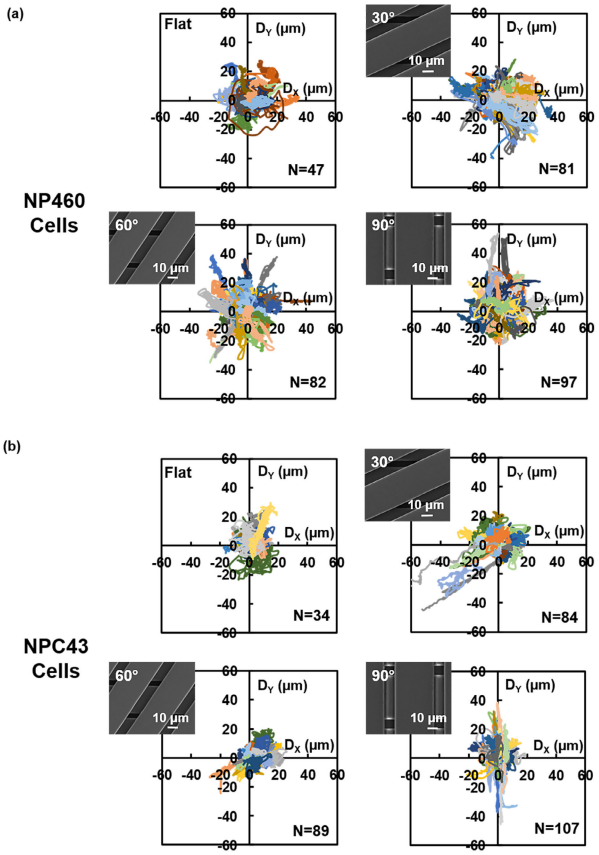

FIGURE 2. Trajectories of (a) NP460 and (b) NPC43 cells on flat and two-layer scaffold platforms with different overlay angles.

The top layers were fixed to 40/10-μm-wide ridges (R)/trenches (T), and the bottom layers were changed from 40/10, 18/18, to 50/50 μm (R/T). In the presence of a 40/10 μm wide (R/T) bottom layer, many NPC43 cells could squeeze into the 10 μm wide top trenches, while only a few NP460 cells could migrate into them. When the bottom layers were 18/18 and 50/50 μm (R/T), both cell lines showed a similar probability of migrating into the 10 μm wide top layers. All the scaffold platforms had a 90° offset angle. In this study, a systematic approach was utilized to investigate how the offset angles between the top and bottom layers influenced NP460 and NPC43 cell separation. Double-layer scaffold platforms were designed with 30°, 60°, and 90° offset angles. Figure 2 shows the NP460 and NPC43 cell migration trajectories. Both cells had random trajectories on the flat PDMS. As shown in Fig. 2(a), NP460 cells displayed the same random movements on the patterned platforms. Therefore, their migration trajectories were independent of the overlaying angles between the two layers. On the contrary, NPC43 cell movements were influenced by the top layer orientation, as shown in Fig. 2(b). The trajectories of NPC43 cells were aligned with the grating orientation of the top layers on the platforms with different overlaying angles.

Based on the cell trajectories, cell migration speed along the x- and y-directions were also calculated, as shown

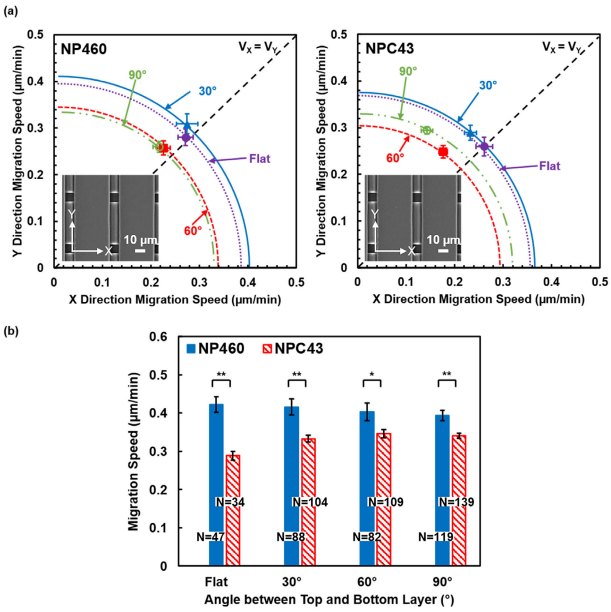

FIGURE 3. **(a) NP460 and NPC43 cell migration directions on flat and two-layer scaffold platforms with different overlay angles. (b) Migration speed of NP460 and NPC43 cells on two-layer scaffold platforms with different overlay angles (*p < 0.05, **p < 0.01, one-way ANOVA with post-hoc tukey HSD test).**

in Fig. 3(a). The diagonal line in the graph indicates equal speed in the x- and y-directions, which represents random cell migration. When the migration speed in the y-direction is faster than in the x-direction, it indicates greater cell migration directionality along the grating orientation on the top layer. The deviation angle measured from the y-axis could be used to express cell migration directionality; the smaller the deviation angle, the stronger the cell migration alignment along the top layer grating. On the flat surface, both NP460 and NPC43 cells migrated randomly with a 45° deviation angle. Very few NP460 cells could migrate from the top layer ridges to the 10 μm wide trenches, and they showed similar random migration on all two-layer platforms with various overlay angles. However, the deviation angle was 39° and 36° for NPC43 cells with some migration guidance when they were on the platforms with 30° and 60° overlays, respectively. The deviation angle was 26° for NPC43 cells on the platforms with 90° overlay angle, indicating stronger guidance along the grating orientation. Therefore, NPC43 cells were better guided by the top layer gratings with increased overlay angle. Typically, a majority of NP460 cells moved randomly on the top layer ridges, and few were guided by the top layer grating. On the other hand, NPC43 cells were better guided by the top layer grating and more cells moved into the 10 μm wide trenches on the top layer. The initial location of cells was also considered. When cells were initially seeded on the top of trenches instead of ridges, they had a higher probability of migrating into the trenches over 16 h. However, even if the initial location of NP460 cells was near the trenches, it was still more difficult for them to squeeze into the trenches compared to NPC43 cells. Lamellipodia, the extended sheet-like membranes of NP460 cells, could not contact the sidewalls of the narrow trenches or the bottom layer as easily as the long protrusions stretched out from NPC43 cells [32].

According to the above results, immortalized NP460 and cancerous NPC43 cells respond differently on the engineered platforms. These findings agreed with a previous study, in which it was found that cells with different metastasis statuses exhibited different migration behaviors when they were seeded on different engineered platforms [24]. Following these findings, cell motility and traversing probability were investigated on these platforms with different overlay angles next.

2) CELL MOTILITY AND MORPHOLOGY OF NP460 AND NPC43 CELLS

The migration speed of NP460 and NPC43 cells over the 16 h imaging time was calculated. Although both NP460 and NPC43 cells showed no significant migration speed dependence with the overlay angle between the top and bottom layers, NPC43 cells moved slightly faster on the scaffold platforms than on the flat PDMS. The enhanced migration speed is most likely due to more cells in the confined trenches that could trigger the regulation of intracellular signaling and morphology changes [35], [44]–[46]. Overall, NP460 cells moved faster than NPC43 cells on all the platforms, as shown in Fig. 3(b). Most NP460 cells stayed on the 40 μm wide top ridges, while many NPC43 cells migrated from the top ridges to the 10 μm wide top layer trenches. This could be further explained by their differing cell morphology [47].

Figure 4(a) shows the scanning electron micrographs of NP460 and NPC43 cells on the top layer ridges. The cell morphology was different between the two cell lines, but independent of the overlay angle between the two layers. In Fig. 4(a), NP460 cells spread on the 40 μm wide ridge with large sheet-like lamellipodia around the cell body. On the other hand, NPC43 cells had more long protrusions stretched out in all directions, as shown in the micrographs. The sheet-like lamellipodia and long protrusions could enhance cell migration as they are rich in myosin II, a motor protein that plays an essential role in cell motility [46].

To quantify the morphological differences of these two cell lines, cell solidity was evaluated. Cell solidity was defined as the actual cell area divided by the convex area of the cell; it is an indicator of the margin undulation of cells. The convex area of a cell is the convex enclosure around the cell perimeter, and it becomes less than one when there are gaps between the convex enclosure and the actual cell perimeter [48]. The actual cell area is indicated with a white line, while the convex area is indicated by a yellow dotted line, as shown in Fig. 4(b). The solidity of NP460 cells was found to be 0.83, larger than a solidity of 0.52 for NPC43 cells. The NP460 cells were more rounded with higher solidity

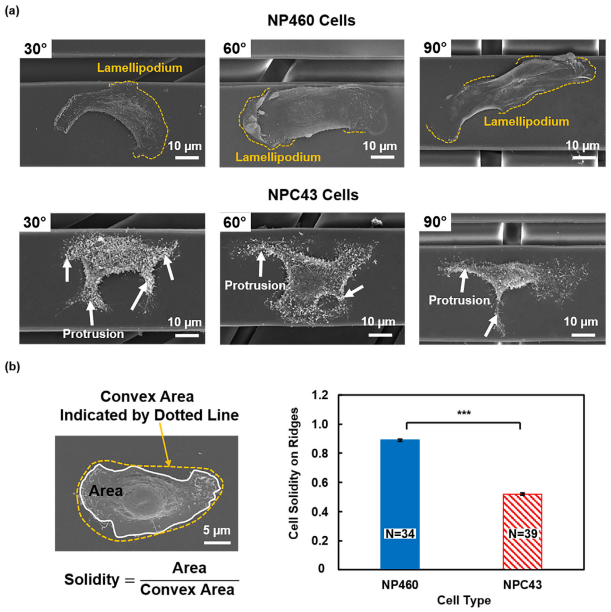

FIGURE 4. (a) Morphologies of NP460 and NPC43 cells on top layer ridges. Yellow dotted lines outlined spreading of lamellipodia of NP460 cells and white arrows represented protrusions of NPC43 cells. (b) Solidity of NP460 and NPC43 cells when they were on the 40 μm ridges (***$p < 0.001$, one-way ANOVA test).

compared to NPC43 cells, which had many long protrusions. The different cell morphologies influenced the cell speed, directionality, and traversing behaviors.

3) OVERLAY ANGLE AFFECTED CELL TRAVERSING BEHAVIORS

Double-layer scaffold platforms with different overlay angles, varying from 30°, 60°, to 90°, were fabricated for cell separation. These engineered platforms were used to represent the ECM in tissue. Typically, the ECM has complex structures, and the overlay angle of the gratings on the scaffold platform can mimic this 3D microenvironment. The different angles between the top and bottom layers provided different surface contact areas for cells to attach and form FAs. The number of cells that moved into the 10 μm wide trenches on the top layer was monitored to calculate the traversing probability as shown in Fig. 5 (a). The traversed cells were defined as cells that stayed in the top layer trenches for more than two-thirds of the entire imaging time. The traversing probability for both NP460 and NPC43 cells increased when the angle between the top and bottom layers increased. For NP460 cells, only a few cells moved into the 10 μm wide top trenches with the probability of 4.2%, 5.5%, and 5.5% at 30°, 60°, and 90° overlay angles, respectively. When NP460 cells were seeded on the platforms, they preferred to stay on the top layer ridges, which is consistent with NP460 cell migration trajectories and directionalities shown in Figs. 2(a) and 3(a), as they were less affected by the offset angles between the top and the bottom layers.

On the contrary, NPC43 cells had higher traversing probability and could migrate from the top layer ridges to the 10 μm wide trenches more easily. The traversing probability was 27.0%, 33.7%, and 66.3% for NPC43 cells when the overlay angles were 30°, 60°, and 90°, respectively. After NPC43 cells moved into the top layer trenches, they migrated along the trench sidewalls and were influenced by the offset angles between the top and the bottom layers. NPC43 cells were more directional, as shown in Fig. 3(a). When the top layer was perpendicular to the bottom layers, it created the smallest non-overlap area by the two gratings. The length of the non-overlap area was 40, 16, and 10 μm as the overlay angle between the top and the bottom layers varied from 30°, 60°, to 90°, respectively. When the top layer was aligned to the bottom layer with a 30° offset, it had the longest distance for the non-overlap areas, which reduced the surface area where cells could contact both adjacent grating as well as the sidewalls of the bottom layers. This reduced surface contact area with the top and bottom layers grating caused a lower probability of cells traversing into the 10 μm wide trenches of the top layer [31], [32].

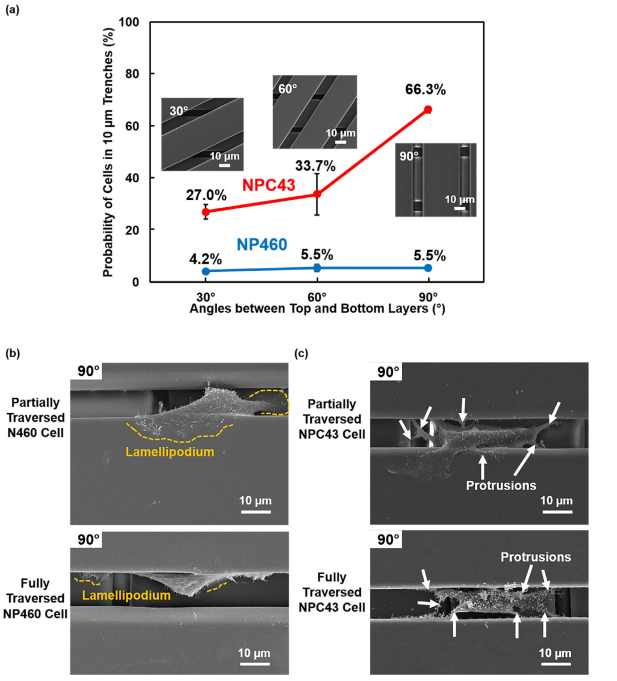

FIGURE 5. (a) Percentage of NP460 and NPC43 cells traversed into 10 μm wide trenches of scaffold platforms with different overlay angles. Cell morphologies of partially and fully traversed (b) NP460 and (c) NPC43 cells on scaffold platforms with 90° overlay angle. Yellow dotted lines outlined spreading of lamellipodia of NP460 cells and white arrows represented protrusions of NPC43 cells.

As NP460 and NPC43 cells behaved differently on such two-layer scaffold platforms, this indicates that it is possible to separate different types of cells. The highest separation efficiency of 92.3% for NPC43 cells was obtained when the top layer was perpendicular to the bottom layer. NP460 cell movement is shown in Supplementary video SV1(a) in the

supporting material. The NP460 cell had a rounded shape at the beginning, and became more elongated as it traversed into the 10 μm wide trenches. Figure 5(b) presents an NP460 cell with its wide lamellipodium extended into the 10 μm wide top trench when trying to squeeze into the trench. After it fully traversed into the top trench, the NP460 cell was elongated along the trench sidewall. On the other hand, the filopodia-like protrusions of NPC43 cell probed around the surrounding environment [49]–[51], as shown in Supplementary video SV1(b). From the micrographs shown in Fig. 5(c), depending on whether the NPC43 cells were partially or fully traversed into the 10 μm wide top trench, the thin and long filopodia-like protrusions sensed and extended around the sidewalls of the top trenches [52]–[54], which made it easier for them to move into the trenches. Therefore, more NPC43 cells with more elongated cell shape and long protrusions were found in the 10 μm wide top trenches.

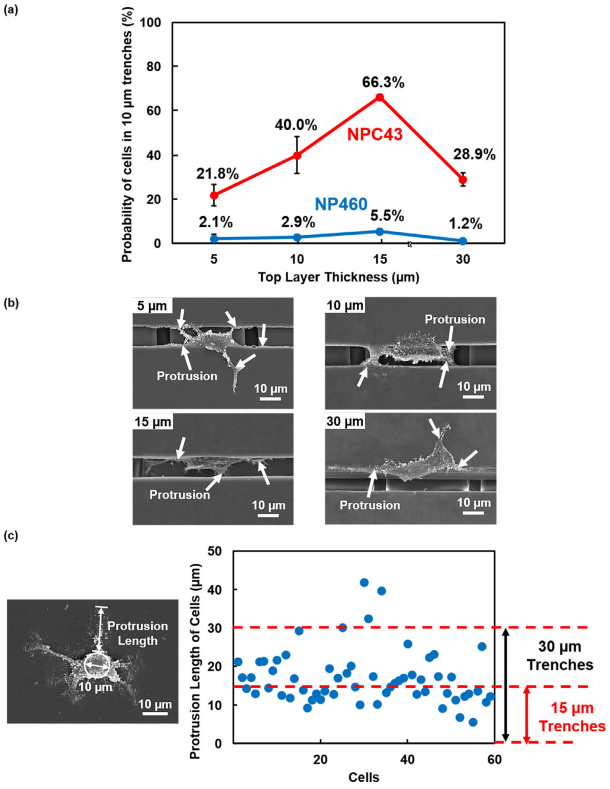

FIGURE 6. (a) Percentage of NP460 and NPC43 cells traversed into 10 μm wide trenches of scaffold platforms with different top layer thicknesses. (b) Micrographs of NPC43 cells traversed into 10 μm wide top layer on two-layer scaffold platforms with different top layer thicknesses. (c) Protrusion length of NPC43 cells when they were on top layer ridges.

C. TWO-LAYER SCAFFOLD PLATFORMS WITH DIFFERENT TOP LAYER THICKNESSES

Following the above results, the angle between the top and bottom layer gratings was fixed to be 90° to achieve the highest traversing probability. To further increase the cell separation efficiency for NPC43 cells, the effects of the top layer thickness on cell migration behaviors were investigated. The depth of the bottom layer was maintained at 15 μm, while the top layer thickness was changed from 5, 10, 15, and 30 μm. The trench depth of the top layer is correlated with the space available for cells to migrate in, which could influence the traversing behaviors of cells [55]. The highest traversing probability was achieved when the top layer was 15 μm deep, with 66.3% for NPC43 cells and 5.5% for NP460 cells, as shown in Fig. 6(a). Thus, the highest separation efficiency reached 92.3%. When the top layer was thinner or thicker than 15 μm, the traversing capability for both NP460 and NPC43 cells dropped. The traversing probability of NPC43 cells was 21.8%, 40.0%, and 28.9% when the top layer thickness was 5, 10, and 30 μm, respectively. Correspondingly, the traversing probability for NP460 cells was 2.1%, 2.9%, and 1.2% for 5, 10, and 30 μm deep top layer trenches. There was minor variation in traversing probability for NP460 cells on platforms with different top layer thicknesses.

Supplementary videos SV2(a-d) in the supporting material show how NPC43 cells moved around top layer trenches when the top layer thickness was varied. Shown in the videos and the micrographs in Fig. 6(b), when the trench depth of the top layer was 5 or 10 μm, which was smaller than the cell size, NPC43 cells migrated directly across the trenches or moved in and out of the trenches because of limited trench depths. The cells could not completely stay in the trenches. In Fig. 6(b), most of the cell bodies were on the top ridges with 5 or 10 μm deep trenches. Thus, the traversing probability for shallow trenches was lower. For 15 μm deep and 10 μm wide trenches on the top layer, cells completely squeezed and stayed in the trenches without any protrusion or cell body on the top ridges. Although deeper trenches of 30 μm for the top layer provided more space in the trenches, it became larger than the typical NPC43 cell size [42]. Cells could not reach the bottom layer and it lowered the traversing probability, as shown in Fig. 6(a). Figure 6(c) shows the protrusion length of NPC43 cells on the top ridges. Out of the 60 cells analyzed, most of them had protrusion lengths less than 30 μm. Therefore, only a few cells could reach the bottom layer grating when the top layer thickness was 30 μm, causing a lower probability for cells to move into the top layer trenches.

D. TWO-LAYER SCAFFOLD PLATFORMS WITH DIFFERENT TOPOGRAPHIES ON BOTTOM LAYER RIDGES

Cells could reach the bottom grating on the double-layer scaffold platform with a 90° overlay angle and 15 μm thick top layer. To modify the surface topography on the bottom layer ridges, a 2/2 μm wide ridge/trench1 μm deep grating was patterned on the bottom layer ridges, parallel to the top layer grating orientation. The effect of surface topography on the bottom layer ridges on cell traversing behaviors was studied. Figure 7 shows that the traversing probability for NP460 cells increased from 5.5% to 7.6%. For NPC43 cells, the traversing

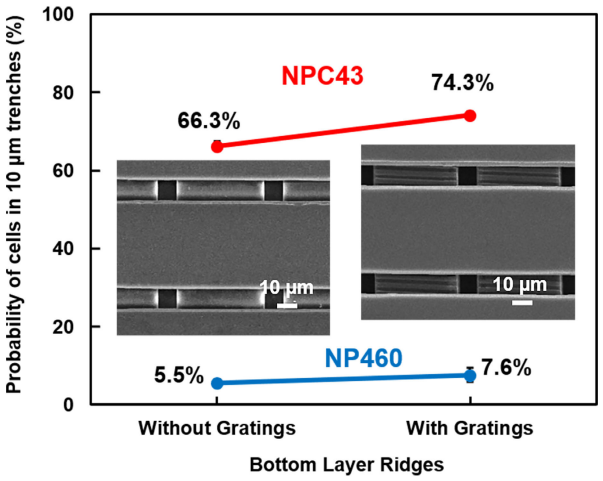

FIGURE 7. Percentage of NP460 and NPC43 cells traversed into 10 μm wide trenches of scaffold platforms with and without gratings on bottom layer ridges.

probability increased from 66.3% to 74.3% when they were seeded on the two-layer scaffold platforms with the top layer grating perpendicular to the bottom layer, a 15 μm thick top layer, and additional grating on the bottom layer ridges that was parallel to the top layer grating orientation. The grating on the bottom layer ridges increased the surface contact area, which promoted cell motility [56], [57]. Previous studies showed that grating patterns increased surface contact area and could guide cell migration. Moreover, the deeper the gratings, the stronger guidance could be obtained [23]. When cells contacted with the additional surface due to the grating pattern on the bottom layer ridges, the coupling produced the traction force to promote cell migration [58].

IV. CONCLUSION

This study utilized designed two-layer scaffold platform in PDMS with different controlled elements to investigate whether different surface contact areas could influence cell migration behaviors. The double-layer scaffold platforms consisted of two 15 μm thick overlying gratings with 40 μm wide ridges and 10 μm wide trenches. NP460 and NPC43 cells were cultured on the patterned platforms for 24 h, and their movements were captured for studying their migration behaviors. The two cell lines migrated differently on the scaffold platforms. NPC43 cells had a stronger reaction to the different scaffold platforms designs compared to NP460 cells. When the overlay angle between the top and bottom layers increased from 30°, 60°, to 90°, the traversing probability also increased from 27.0%, 33.7%, to 66.3% for NPC43 cells. Correspondingly, the traversing probability for NP460 cells was 4.2%, 5.5%, and 5.5%. 66.3% of NPC43 cells and 5.5% of NP460 cells could stay in the top layer trenches when the top layer was 15 μm thick. Furthermore, when the top layers were too small or too large compared to the cell size, it was more difficult for them to stay and squeeze in the top layer trenches. Introducing shallow grating structures on the bottom layer ridges attracted more NP460 and NPC43 cells to move into the 10 μm wide top trenches. The traversing probability increased from 5.5% to 7.6% for NP460 cells, and 66.3% to 74.3% for NPC43 cells. The highest efficiency of separating NPC43 cells from NP460 cells was 92.3%, which was achieved by the top layer grating being perpendicular to the bottom layer, a 15 μm thick top layer, and 1 μm deep gratings on the bottom layer ridges. These results showed that NPC43 cells could be effectively separated from NP460 cells on the proposed platforms. If NPC43 cells are isolated, high throughput drug screening could potentially be implemented for early diagnosis and treatment of NPC.

ACKNOWLEDGMENT

The authors acknowledge Prof. S. W. Tsao and Prof. C. M. Tsang from the School of Biomedical Science, The University of Hong Kong, for providing the cell line studied in this project. They appreciate the technical support from the staff at the Centre for Biosystems, Neuroscience, and Nanotechnology, City University of Hong Kong.

AUTHOR CONTRIBUTIONS

Muting Wang and Stella W. Pang designed the research; Muting Wang fabricated the platforms, carried out the biological experiments, and analyzed the data; Stella W. Pang supervised the project and provided the resources; Muting Wang and Stella W. Pang wrote the article and reviewed the manuscript.

CONFLICT OF INTERESTS

There are no conflicts to declare.

REFERENCES

[1] H. Sung, J. Ferlay, R. L. Siegel, M. Laversanne, I. Soerjomataram, A. Jemal, and F. Bray, "Global cancer statistics 2020: GLOBOCAN estimates of incidence and mortality worldwide for 36 cancers in 185 countries," *CA, Cancer J. Clin.*, vol. 71, no. 3, pp. 209–249, Feb. 2021, doi: 10.3322/caac.21660.

[2] D.-H. Lee, X. Li, N. Ma, M. A. Digman, and A. P. Lee, "Rapid and label-free identification of single leukemia cells from blood in a high-density microfluidic trapping array by fluorescence lifetime imaging microscopy," *Lab Chip*, vol. 18, no. 9, pp. 1349–1358, 2018, doi: 10.1039/C7LC01301A.

[3] P. S. Sankar, M. F. C. Mat, K. Muniandy, B. L. S. Xiang, P. S. Ling, S. L. L. Hoe, A. S.-B. Khoo, and N. Mohana-Kumaran, "Modeling nasopharyngeal carcinoma in three dimensions," *Oncol. Lett.*, vol. 13, no. 4, pp. 2034–2044, Feb. 2017, doi: 10.3892/ol.2017.5697.

[4] Y. Zhao, D. Xu, and W. Tan, "Aptamer-functionalized nano/micromaterials for clinical diagnosis: Isolation, release and bioanalysis of circulating tumor cells," *Integrative Biol.*, vol. 9, no. 3, pp. 188–205, 2017, doi: 10.1039/c6ib00239k.

[5] W. I. Wei and J. S. Sham, "Nasopharyngeal Carcinoma," *Lancet*, vol. 365, no. 9476, pp. 2041–2054, Jun. 2005, doi: 10.1016/S0140-6736(05)66698-6.

[6] A. S. C. Chan, K. F. To, K. W. Lo, K. F. Mak, W. Pak, B. Chiu, M. Gary, M. Ding, X. Li, and J. C. K. Lee, "High frequency of chromosome 3p deletion in histologically normal nasopharyngeal epithelia from southern Chinese," *Cancer Res.*, vol. 60, no. 19, pp. 5365–5370, Oct. 2000.

[7] S. W. Tsao, Y. L. Yip, C. M. Tsang, P. S. Pang, V. M. Y. Lau, G. Zhang, and K. W. Lo, "Etiological factors of nasopharyngeal carcinoma," *Oral Oncol.*, vol. 50, no. 5, pp. 330–338, May 2014, doi: 10.1016/j.oraloncology.2014.02.006.

[8] W. T. Ng, K. T. Yuen, K. H. Au, O. S. H. Chan, and A. W. M. Lee, "Staging of nasopharyngeal carcinoma–the past, the present and the future," *Oral Oncol.*, vol. 50, no. 6, pp. 549–554, Jun. 2014, doi: 10.1016/j.oraloncology.2013.06.003.

[9] K. W. Lo, K. F. To, and D. P. Huang, "Focus on nasopharyngeal carcinoma," *Cancer Cell*, vol. 5, no. 5, pp. 423–428, Jun. 2004, doi: 10.1016/S1535-6108(04)00119-9.

[10] S. Sinha and A. Gajra, "Nasopharyngeal cancer," in *Statpearls*. Treasure Island, FL, USA: StatPearls, 2020. [Online]. Available: https://www.ncbi.nlm.nih.gov/books/NBK459256/

[11] B. P. Lam, S. K. C. Cheung, Y. W. Lam, and S. W. Pang, "Microenvironmental topographic cues influence migration dynamics of nasopharyngeal carcinoma cells from tumour spheroids," *RSC Adv.*, vol. 10, no. 48, pp. 28975–28983, Aug. 2020, doi: 10.1039/D0RA03740K.

[12] C. M. Tsang, Z. Y. Liu, W. Zhang, C. You, G. E. Jones, S. W. Tsao, and S. W. Pang, "Integration of biochemical and topographic cues for the formation and spatial distribution of invadosomes in nasopharyngeal epithelial cells," *Acta Biomater.*, vol. 101, pp. 168–182, Jan. 2020, doi: 10.1016/j.actbio.2019.10.043.

[13] F. Zhang and J. Zhang, "Clinical hereditary characteristics in nasopharyngeal carcinoma through Ye-Liang's family cluster," *Chin. Med. J.*, vol. 112, no. 2, pp. 185–187, Feb. 1999.

[14] S. Tsao, C. M. Tsang, K. To, and K. Lo, "The role of Epstein–Barr virus in epithelial malignancies," *J. Pathol.*, vol. 235, no. 2, pp. 323–333, Jan. 2015, doi: 10.1002/path.4448.

[15] S. Y.-Y. Chan, K.-W. Choy, S.-W. Tsao, Q. Tao, T. Tang, G. T.-Y. Chung, and K.-W. Lo, "Authentication of nasopharyngeal carcinoma tumor lines," *Int. J. Cancer*, vol. 122, no. 9, pp. 2169–2171, Jan. 2008, doi: 10.1002/ijc.23374.

[16] H.-C. Wu, Y.-J. Lin, J.-J. Lee, Y.-J. Liu, S.-T. Liang, Y. Peng, Y.-W. Chiu, C.-W. Wu, and C.-T. Lin, "Functional analysis of EBV in nasopharyngeal carcinoma cells," *Lab. Invest.*, vol. 83, no. 6, pp. 797–812, Jun. 2003.

[17] H. Pertoft, "Fractionation of cells and subcellular particles with Percoll," *J. Biochem. Biophys. Methods*, vol. 44, nos. 1–2, pp. 1–30, Jul. 2000, doi: 10.1016/s0165-022x(00)00066-x.

[18] L. A. Herzenberg, D. Parks, B. Sahaf, O. Perez, M. Roederer, and L. A. Herzenberg, "The history and future of the fluorescence activated cell sorter and flow cytometry: A view from Stanford," *Clin. Chem.*, vol. 48, no. 10, pp. 1819–1827, Oct. 2002, doi: 10.1093/clinchem/48.10.1819.

[19] I. Šafařík and M. Šafaříková, "Use of magnetic techniques for the isolation of cells," *J. Chromatogr. B, Biomed. Sci. Appl.*, vol. 722, pp. 33–53, Feb. 1999.

[20] A. A. S. Bhagat, H. Bow, H. W. Hou, S. J. Tan, J. Han, and C. T. Lim, "Microfluidics for cell separation," *Med. Biol. Eng. Comput.*, vol. 48, no. 10, pp. 999–1014, Oct. 2010, doi: 10.1007/s11517-010-0611-4.

[21] R. Horwitz and D. Webb, "Cell migration," *Current Biol.*, vol. 13, no. 19, pp. R756–R759, Sep. 2003, doi: 10.1016/j.cub.2003.09.014.

[22] M. Vicente-Manzanares and A. R. Horwitz, "Cell migration: An overview," *Cell Migration*, vol. 769, pp. 1–24, Oct. 2011, doi: 10.1007/978-1-61779-207-6_1.

[23] F. M. Refaaq, X. Chen, and S. W. Pang, "Effects of topographical guidance cues on osteoblast cell migration," *Sci. Rep.*, vol. 10, no. 1, Nov. 2020, Art. no. 20003, doi: 10.1038/s41598-020-77103-0.

[24] S. F. Zhou, S. Gopalakrishnan, Y. H. Xu, S. K. Y. To, A. S. T. Wong, S. W. Pang, and Y. W. Lam, "Substrates with patterned topography reveal metastasis of human cancer cells," *Biomed. Mater.*, vol. 12, no. 5, Aug. 2017, Art. no. 055001, doi: 10.1088/1748-605X/aa785d.

[25] A. T. Nguyen, S. R. Sathe, and E. K. F. Yim, "From nano to micro: Topographical scale and its impact on cell adhesion, morphology and contact guidance," *J. Phys., Condens. Matter*, vol. 28, no. 18, May 2016, Art. no. 183001, doi: 10.1088/0953-8984/28/18/183001.

[26] S. F. Zhou, S. Gopalakrishnan, Y. H. Xu, J. Yang, Y. W. Lam, and S. W. Pang, "A unidirectional cell switching gate by engineering grating length and bending angle," *PLoS ONE*, vol. 11, no. 1, Jan. 2016, Art. no. e0147801, doi: 10.1371/journal.pone.0147801.

[27] Q. Y. Tang, W. X. Qian, Y. H. Xu, S. Gopalakrishnan, J. Q. Wang, Y. W. Lam, and S. W. Pang, "Control of cell migration direction by inducing cell shape asymmetry with patterned topography," *J. Biomed. Mater. Res. A*, vol. 103, no. 7, pp. 2383–2393, Jul. 2015, doi: 10.1002/jbm.a.35378.

[28] Q. Y. Tang, W. Y. Tong, J. Shi, P. Shi, Y. W. Lam, and S. W. Pang, "Influence of engineered surface on cell directionality and motility," *Biofabrication*, vol. 6, no. 1, Mar. 2014, Art. no. 015011, doi: 10.1088/1758-5082/6/1/015011.

[29] C. T. McKee, J. A. Wood, I. Ly, P. Russell, and C. J. Murphy, "The influence of a biologically relevant substratum topography on human aortic and umbilical vein endothelial cells," *Biophys. J.*, vol. 102, no. 5, pp. 1224–1233, Mar. 2012, doi: 10.1016/j.bpj.2012.01.053.

[30] P. Clark, P. Connolly, A. S. Curtis, J. A. Dow, and C. D. Wilkinson, "Cell guidance by ultrafine topography *in vitro*," *J. Cell Sci.*, vol. 99, no. 1, pp. 73–77, May 1991, doi: 10.1242/jcs.99.1.73.

[31] Z. Liu, W. Zhang, and S. W. Pang, "Migration of immortalized nasopharyngeal epithelia and carcinoma cells through porous membrane in 3D platforms," *Biosci. Rep.*, vol. 40, no. 6, Jun. 2020, Art. no. BSR20194113, doi: 10.1042/bsr20194113.

[32] W. G. Zhang, Z. Y. Liu, and S. W. Pang, "Separation of nasopharyngeal epithelial cells from carcinoma cells on 3D scaffold platforms," *Biotechnol. Bioeng.*, vol. 118, no. 4, pp. 1444–1455, Apr. 2021, doi: 10.1002/bit.27640.

[33] P. Tayalia, C. R. Mendonca, T. Baldacchini, D. J. Mooney, and E. Mazur, "3D cell-migration studies using two-photon engineered polymer scaffolds," *Adv. Mater.*, vol. 20, no. 23, pp. 4494–4498, Dec. 2008, doi: 10.1002/adma.200801319.

[34] A. J. Ridley, M. A. Schwartz, R. A. Firtel, M. H. Ginsberg, G. Borisy, J. T. Parsons, A. R. Horwitz, and K. Burridge, "Cell migration: Integrating signals from front to back," *Science*, vol. 302, no. 5651, pp. 1704–1709, 2003, doi: 10.1126/science.1092053.

[35] B. P. Lam, Y. W. Lam, and S. W. Pang, "Using biomimetic scaffold platform to detect growth factor induced changes in migration dynamics of nasopharyngeal epithelial cells," *IEEE Access*, vol. 8, pp. 187553–187563, 2020, doi: 10.1109/ACCESS.2020.3030953.

[36] F. Travascio, *Composition and Function of the Extracellular Matrix in the Human Body*. London, U.K.: IntechOpen, 2016.

[37] J. Nicolas, S. Magli, L. Rabbachin, S. Sampaolesi, F. Nicotra, and L. Russo, "3D extracellular matrix mimics: Fundamental concepts and role of materials chemistry to influence stem cell fate," *Biomacromolecules*, vol. 21, no. 6, pp. 1968–1994, Mar. 2020, doi: 10.1021/acs.biomac.0c00045.

[38] B. Jing, Y. Luo, B. Lin, J. Li, Z. A. Wang, and Y. Du, "Establishment and application of a dynamic tumor-vessel microsystem for studying different stages of tumor metastasis and evaluating anti-tumor drugs," *RSC Adv.*, vol. 9, no. 30, pp. 17137–17147, May 2019, doi: 10.1039/C9RA02069A.

[39] X. Ma, J. Liu, W. Zhu, M. Tang, N. Lawrence, C. Yu, M. Gou, and S. Chen, "3D bioprinting of functional tissue models for personalized drug screening and *in vitro* disease modeling," *Adv. Drug Del. Rev.*, vol. 132, pp. 235–251, Jul. 2018, doi: 10.1016/j.addr.2018.06.011.

[40] E. Tomecka, K. Zukowski, E. Jastrzebska, M. Chudy, and Z. Brzozka, "Microsystem with micropillar array for three-(gel-embaded) and two-dimensional cardiac cell culture," *Sens. Actuators B, Chem.*, vol. 254, pp. 973–983, Jan. 2018, doi: 10.1016/j.snb.2017.07.186.

[41] D. Kloß, R. Kurz, H.-G. Jahnke, M. Fischer, A. Rothermel, U. Anderegg, J. C. Simon, and A. A. Robitzki, "Microcavity array (MCA)-based biosensor chip for functional drug screening of 3D tissue models," *Biosensors Bioelectron.*, vol. 23, no. 10, pp. 1473–1480, May 2008, doi: 10.1016/j.bios.2008.01.003.

[42] A. C. Romano, E. M. Espana, S. H. Yoo, M. T. Budak, J. M. Wolosin, and S. C. Tseng, "Different cell sizes in human limbal and central corneal basal epithelia measured by confocal microscopy and flow cytometry," *Invest. Ophthalmol. Vis. Sci.*, vol. 44, no. 12, pp. 5125–5129, Dec. 2003, doi: 10.1167/iovs.03-0628.

[43] W. G. Zhang, Z. Y. Liu, and S. W. Pang, "Effects of three-dimensional platform stiffness and layer dimensions on separation of carcinoma cells," *Engineering*, Nov. 2020, doi: 10.1016/j.eng.2020.09.010.

[44] C.-Y. Liu, H.-H. Lin, M.-J. Tang, and Y.-K. Wang, "Vimentin contributes to epithelial-mesenchymal transition cancer cell mechanics by mediating cytoskeletal organization and focal adhesion maturation," *Oncotarget*, vol. 6, no. 18, pp. 15966–15983, Jun. 2015, doi: 10.18632/oncotarget.3862.

[45] A. Pathak and S. Kumar, "Independent regulation of tumor cell migration by matrix stiffness and confinement," *Proc. Nat. Acad. Sci. USA*, vol. 109, no. 26, pp. 10334–10339, Jun. 2012, doi: 10.1073/pnas.1118073109.

[46] B. Geiger, J. P. Spatz, and A. D. Bershadsky, "Environmental sensing through focal adhesions," *Nature Rev. Mol. Cell Biol.*, vol. 10, pp. 21–33, Jan. 2009, doi: 10.1038/nrm2593.

[47] Y.-J. Liu, M. Le Berre, F. Lautenschlaeger, P. Maiuri, A. Callan-Jones, M. Heuzé, T. Takaki, R. Voituriez, and M. Piel, "Confinement and low adhesion induce fast amoeboid migration of slow mesenchymal cells," *Cell*, vol. 160, no. 4, pp. 659–672, Feb. 2015, doi: 10.1016/j.cell.2015.01.007.
[48] R. V. Vőfély, J. Gallagher, G. D. Pisano, M. Bartlett, and S. A. Braybrook, "Of puzzles and pavements: A quantitative exploration of leaf epidermal cell shape," *New Phytologist*, vol. 221, no. 1, pp. 540–552, Jan. 2019, doi: 10.1111/nph.15461.
[49] P. K. Mattila and P. Lappalainen, "Filopodia: Molecular architecture and cellular functions," *Nature Rev. Mol. Cell Biol.*, vol. 9, no. 6, pp. 446–454, 2008, doi: 10.1038/nrm2406.
[50] X.-B. Yuan, M. Jin, X. Xu, Y.-Q. Song, C.-P. Wu, M.-M. Poo, and S. Duan, "Signalling and crosstalk of Rho GTPases in mediating axon guidance," *Nature Cell Biol.*, vol. 5, no. 1, pp. 38–45, Jan. 2003, doi: 10.1038/ncb895.
[51] R. W. Davenport, P. Dou, V. Rehder, and S. B. Kater, "A sensory role for neuronal growth cone filopodia," *Nature*, vol. 361, no. 6414, pp. 721–724, Feb. 1993.
[52] M. B. Steketee and K. W. Tosney, "Three functionally distinct adhesions in filopodia: Shaft adhesions control lamellar extension," *J. Neurosci.*, vol. 22, no. 18, pp. 8071–8083, Sep. 2002, doi: 10.1523/JNEUROSCI.22-18-08071.2002.
[53] M. P. Sheetz, N. L. Baumrind, D. B. Wayne, and A. L. Pearlman, "Concentration of membrane antigens by forward transport and trapping in neuronal growth cones," *Cell*, vol. 61, no. 2, pp. 231–241, Apr. 1990, doi: 10.1016/0092-8674(90)90804-N.
[54] P. C. Letourneau and T. A. Shattuck, "Distribution and possible interactions of actin-associated proteins and cell adhesion molecules of nerve growth cones," *Development*, vol. 105, no. 3, pp. 505–519, Mar. 1989, doi: 10.1242/dev.105.3.505.
[55] Z. Y. Liu, W. G. Zhang, and S. W. Pang, "Traversing behavior of tumor cells in three-dimensional platforms with different topography," *PLoS ONE*, vol. 15, no. 6, Jun. 2020, Art. no. e0234482, doi: 10.1371/journal.pone.0234482.
[56] F. Gentile, L. Tirinato, E. Battista, F. Causa, C. Liberale, E. M. di Fabrizio, and P. Decuzzi, "Cells preferentially grow on rough substrates," *Biomaterials*, vol. 31, no. 28, pp. 7205–7212, Oct. 2010, doi: 10.1016/j.biomaterials.2010.06.016.
[57] C. Galli, G. Passeri, F. Ravanetti, E. Elezi, M. Pedrazzoni, and G. M. Macaluso, "Rough surface topography enhances the activation of Wnt/β-catenin signaling in mesenchymal cells," *J. Biomed. Mater. Res. A*, vol. 95A, no. 3, pp. 682–690, Dec. 2010, doi: 10.1002/jbm.a.32887.
[58] P. Lamoureux, R. E. Buxbaum, and S. R. Heidemann, "Direct evidence that growth cones pull," *Nature*, vol. 340, no. 6229, pp. 159–162, Jul. 1989, doi: 10.1038/340159a0.

MUTING WANG received the M.S. degree in electronics from The Chinese University of Hong Kong, China. She is currently pursuing the Ph.D. degree with the Department of Electrical Engineering, City University of Hong Kong. Her research interests include nanotechnology, cell migration, and cell separation.

STELLA W. PANG (Fellow, IEEE) received the B.Sc. degree from Brown University, Providence, RI, USA, in 1977, and the M.Sc. and Ph.D. degrees from Princeton University, Princeton, NJ, USA, in 1978 and 1981, respectively.

From 1981 to 1989, she was with Lincoln Laboratory, Massachusetts Institute of Technology, Cambridge, MA, USA. From 1990 to 2011, she was a Professor of electrical engineering and computer science and the Associate Dean of the Graduate Education and International Programs with the College of Engineering, University of Michigan, Ann Arbor, MI, USA, from 2002 to 2007. She is currently a Chair Professor and the Head of the Department of Electrical Engineering, City University of Hong Kong, Hong Kong, where she is also the Director of the Center for Biosystems, Neuroscience, and Nanotechnology. She has over 400 technical articles, book chapters, and invited presentations. She is an editor and the author of 16 books, journals, and conference proceedings. She has nine patents granted in nanotechnology and microsystems. She has taught 32 short courses on microfabrication and nanoimprint technology for microelectronic manufacturing and microelectromechanical systems. Her research interests include nanofabrication technology for biomedical, microelectromechanical, microelectronic, and optical devices.

Prof. Pang is a fellow of the Electrochemical Society (ECS), the American Vacuum Society (AVS), and Hong Kong Institution of Engineers (HKIE). She has served as the Conference Organizer for AVS, ECS, the IEEE Electronic Materials Conference, the International Symposium on Electron, Ion, and Photon Beam Technology, and Nanofabrication, the Material Research Society, and SPIE.